J. Electrochem. Sci. Eng. **15(4)** (2025) 2769; http://dx.doi.org/10.5599/jese.2769

Open Access : : ISSN 1847-9286
www.jESE-online.org

Original scientific paper

Aminopyridine Schiff bases as eco-friendly corrosion inhibitors for carbon steel in acidic media: experimental and quantum chemical insights

Shereen M. Al-Shomar[1], Ahmed A. Farag[2,✉], Fekhra Hedhili[1], Hissah Saedoon Albaqawi[1], Nwuyer A. Al-Shammari[1], Khaled M. Abdel-Azim[3] and Nashwa S. Abdelshafi[3]

[1]*Department of Physics, College of Science, University of Ha'il, P.O. Box 2440, Ha'il, Saudi Arabia*
[2]*Egyptian Petroleum Research Institute (EPRI), Nasr City, 11727 Cairo, Egypt*
[3]*Chemistry Department, Faculty of Education, Ain Shams University, Roxy, Cairo 11711, Egypt*

Corresponding author: ✉ *ahmedafm@yahoo.com; Tel.: 01009270941*

Received: April 22, 2025; Accepted: June 9, 2025; Published: June 13, 2025

Abstract

Material degradation has received a lot of attention from the scientific community as a serious problem. However, a major barrier to the application of effective corrosion treatment is the ban on the use of inhibitors containing dangerous substances. In addition to being efficient corrosion inhibitors, Schiff bases offer pharmacological, anti-inflammatory, antibacterial, anti-cancer, and antioxidant qualities. In this experiment, two types of aminopyridine Schiff bases were used to investigate the corrosion resistance of carbon steel (C-steel) in an environment containing 1 mol L^{-1} HCl. The study used weight loss and electrochemical assays to assess the corrosion-inhibiting effectiveness of two Schiff base derivatives (HAPT and HHTA). It was found that the inhibitory efficiency rises with increasing HAPT and HHTA dosages and falls with increasing temperature. HAPT and HHTA showed impressive corrosion inhibition rates of 93.4 and 95.2 %, respectively. The enhanced inhibitory efficiency results from the significant adsorption of HAPT and HHTA molecules on the C-steel surface through chemisorption and physisorption in compliance with the Langmuir adsorption isotherm. The production of an inhibitory film on the C-steel substrate was confirmed by the results of the scanning electron microscope. Density functional theory and molecular dynamics computations in quantum chemistry were used to identify the adsorption of HAPT and HHTA at the steel/solution interface.

Keywords

Metal alloy; acid corrosion; aminopyridine inhibitors; electrochemical testing; weight loss; quantum chemical calculations

Introduction

Carbon steel (C-steel) is a widely used alloy in industries such as machine tools, chemicals, and construction [1,2]. However, it is prone to corrosion in its abundance of hydrogen ions. Pickling, industrial washing, descaling, oil well acidizing, and the petrochemical sector are all examples of industries that routinely use acid solutions [3]. Nevertheless, the use of such improvements may cause corrosion harm to C-steel [4]. Slowing the progress of corrosion of C-steel in acidic environments is critical for reducing worldwide economic losses and avoiding safety incidents caused by metal failure [5]. As a result, in order to employ C-steel in production, it is critical to prevent corrosion in acidic environments [6]. Industry researchers and academics have investigated a variety of corrosion-prevention strategies [7]. One of the most prevalent approaches is to add corrosion inhibitors to solutions with acidity. While they are widely utilized due to their efficacy, some highly hazardous inhibitors do not meet environmental standards [8]. As a result, it is critical to create eco-friendly alternatives to safeguard C-steel from corrosion in acidic environments [9]. In previous times, corrosion inhibitors were mostly inorganic compounds. However, as the worldwide focus on sustainable development grows, research on non-toxic corrosion inhibitors has expanded. As the research developed, it became obvious that the majority of inorganic inhibiting agents for corrosion are very hazardous and carcinogenic, limiting their continued usage. Organic inhibitors, on the other hand, adhere to the rules of sustainable development, making them a more environmentally responsible option [10]. These corrosion inhibitors typically contain heteroatoms as well as unsaturated bonding, and aromatic ring atoms with symmetrical conjugated frameworks in their chemical makeup. These structural components contain lone pairs of electric charges that enable the inhibitor to connect to the iron's *d*-orbitals, allowing it to firmly attach to the steel surface. Organic corrosion inhibitors are classified into several types, which include triazine, imidazole, pyridine, Mannich reaction, and others. It should be noted that one of the key characteristics that sets heterocyclic organic inhibitors apart from others is the presence of certain electron-donating atoms, such as oxygen, sulphur, and nitrogen, which enable them to spontaneously adsorb onto the metal's surface and create a barrier against corrosion. Pyridine compounds, notably their Schiff bases, are a highly relevant class of heterocycles that have sparked considerable curiosity in the pharmaceutical and chemical industries [11]. They are described, along with their synthesis, in a variety of writings and studies [12]. Organic compounds, particularly Schiff bases, have lately been investigated as corrosion inhibitors for various alloys and metals in acidic environments, with several of them being cited as promising corrosion inhibitors for C-steel [13]. These chemicals are adsorbed on the metal's surface, preventing active corrosion. Some documented studies demonstrate that the efficiency of Schiff base inhibition is significantly higher than that of aldehydes and related amines, which could be attributed to the existence of the imine group -C=N- in those compounds [14].

Aminopyridines belong to the family of monoamino and diamino pyridine derivatives. It is essential to medicine, pharmacology, and biology. Aminopyridine also showed remarkable stability, reusing up to four times without experiencing appreciable deterioration. This strategy works especially well for solving environmental problems and meeting business needs. The use of aminopyridines, incorporating heterocyclic atoms in addition to the Schiff base's azomethine group, as steel corrosion inhibitors in acidic media is innovative in this context [15].

Quantum chemistry calculations are commonly used to predict the connection mechanism between corrosion inhibitors and metal surfaces and to pinpoint active inhibitor sites. Thus, it has been observed that corrosion inhibition efficiency is determined by the physicochemical and electrical features of organic inhibitors, in addition to the contact between the inhibitors and the

surface of the metal [16]. These theoretical investigations provide access to various quantum metrics of organic entities, specifically frontier molecular orbitals and charges, which are commonly utilized to determine molecule reactivity.

In the current work, two aminopyridine Schiff base derivatives, (E)-6-((4-hydroxybenzylidene)amino)pyridine-2(1H)-thione (HAPT) and (Z)-2-hydroxy-2-(4-hydroxyphenyl)-N-(6-thioxo-1,6-dihydropyridin-2-yl)acetimidic acid (HHTA) were easily synthesized in a single step (condensation reaction) and has good solubility in polar solvents such as water, methanol, ethanol, and acetone. HAPT and HHTA, which contain thione, hydroxyl, amino groups, aromatic rings, and imine bonds characteristic of Schiff base compounds, were used as corrosion inhibitors for C-steel in 1 mol L^{-1} HCl solution. HAPT and HHTA's mitigating effects were assessed utilizing chemical and electrochemical methodologies. Finally, the corrosion protection of C-steel surfaces with HAPT and HHTA was studied using density functional theory (DFT) and molecular dynamics (MD) simulation, as well as the surface morphological analysis using a scanning electron microscope (SEM).

Experimental

Materials and solutions

The C-steel specimens utilized in this study have the following composition: 0.08 % P, 0.01 % Cr, 0.35 % Si, 0.08 % Mn, 0.21 % C, 0.07 % S, and the remainder iron. Analytical grade HCl (37 % dilution with bi-distilled water) was used to create the 1 mol L^{-1} HCl solution. Next, produce HAPT and HHTA solutions with concentrations ranging from 0.5 to 1.0 mmol L^{-1}. Sigma-Aldrich provided the synthesis reagents for 6-aminopyridine-2(1H)-thione, 4-hydroxybenzaldehyde, and 2-hydroxy-2-(4-hydroxyphenyl)acetic. The suppliers of acetone, ethanol, and hydrochloric acid were El Gomhoureya for Drugs Trade & Medical Supplies, Egypt. The synthesized chemical components were dissolved in the aggressive electrolyte created to provide a range of dosages from 0.05 to 1.00 mM, which was needed to construct HAPT and HHTA inhibitors.

Synthesis of inhibitors

The preparation way for the Schiff bases (E)-6-((4-hydroxybenzylidene)amino)pyridine-2(1H)-thione (HAPT) and (Z)-2-hydroxy-2-(4-hydroxyphenyl)-N-(6-thioxo-1,6-dihydropyridin-2-yl)acetimidic acid (HHTA) is given in Figure 1.

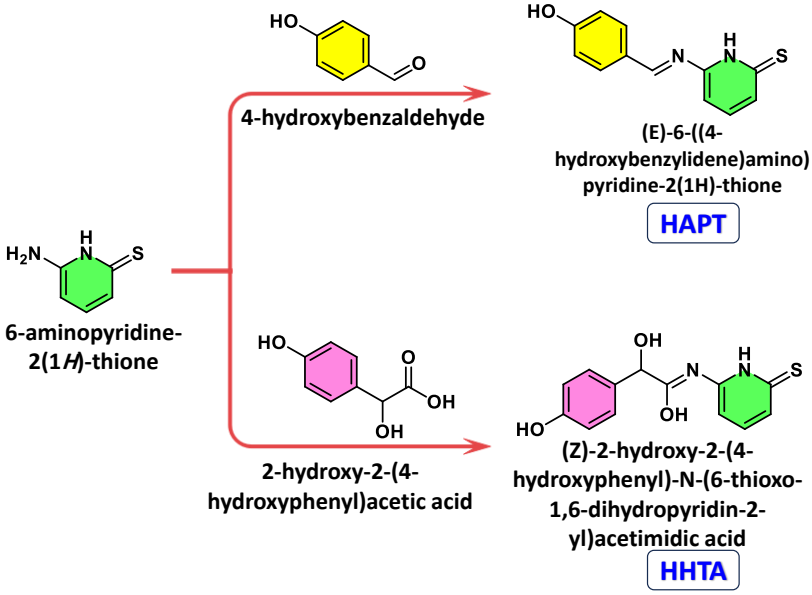

Figure 1. *Schematic of the synthesis of the HAPT and HHTA*

4-hydroxybenzaldehyde (2.442 g, 20 mM) or 2-hydroxy-2-(4-hydroxyphenyl)acetic acid (3.363 g, 20 mM) in 20 mL ethanol was added to an ethanolic solution of 6-aminopyridine-2(1H)-thione (2.524 g, 20 mM). For six hours at 60 °C, the solution was refluxed using a condensation procedure with a minor amount of para-toluene sulfonic acid (PTSA) present as a catalyst. The reaction mixture was transferred to a beaker and allowed to come to room temperature. The distilled water wash and vacuum drying, followed by several ethanolic washes to eliminate unreacted compounds, were performed on the solidified Schiff bases, HAPT and HHTA. The chart analysis of FTIR and ^{1}H NMR for both HAPT and HHTA Schiff bases is given in Figures 2(a) and 2(b), respectively.

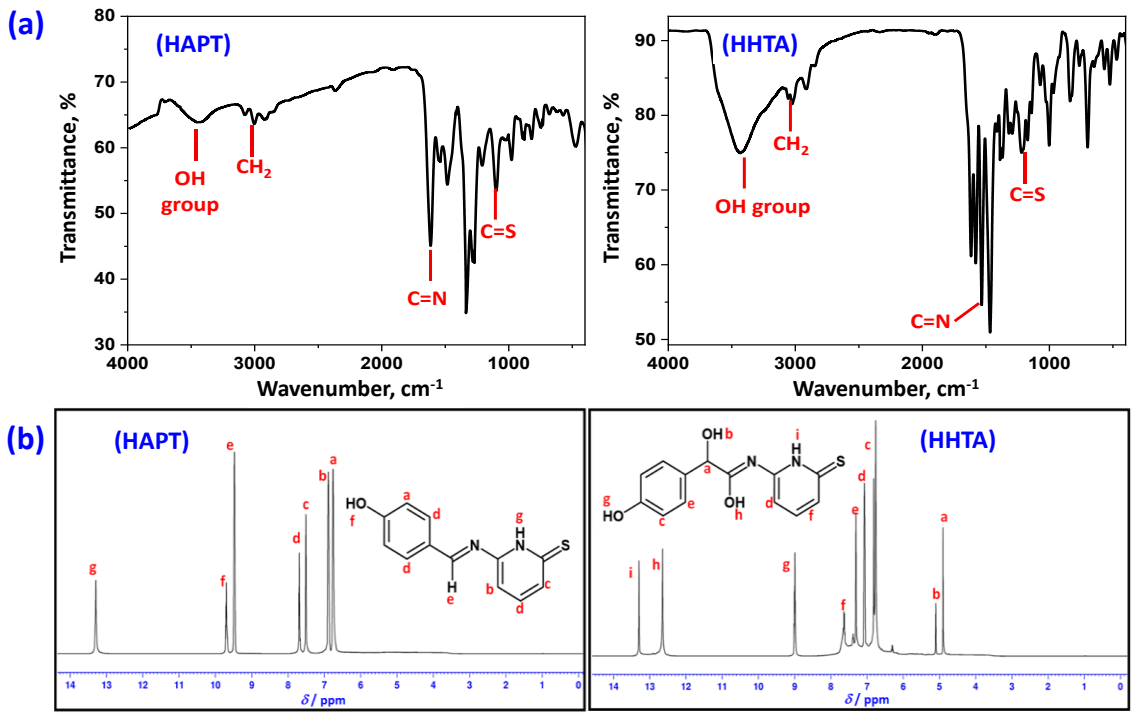

Figure 2. *(a) FTIR and (b) ^{1}H NMR charts of HAPT and HHTA Schiff bases*

(E)-6-((4-hydroxybenzylidene)amino)pyridine-2(1H)-thione (HAPT)

Yield: 82 %. M.p. 171 °C; ^{1}H NMR; δH (500 MHz; DMSO-*d6*; 293 K): 6.81 (m, 2H, 2 aromatic CH adjacent to OH group of phenol ring), 6.95 (dd, *J* = 8.4, 1.5 Hz, 1H, aromatic CH of pyridine-2(1H)--thione ring adjacent to C-N=C group), 7.61 - 7.51 (m, 3H), 7.52 (H, aromatic CH of pyridine-2(1H)--thione ring adjacent to C=S group), 7.59 (H, aromatic CH of pyridine-2(1H)-thione ring), 7.67 (H, aromatic CH of phenol ring), 9.48 (H, CH of imine group), 9.71 (s, 1H, OH group), 13.68 (s, 1H, NH group); Elemental analysis: C, 62.59; H, 4.38; N, 12.16; O, 6.95; S, 13.92; IR: Stretching vibration of the hydroxyl groups was identified as the cause of a large absorption peak at 3430 to 3435 cm^{-1}. The absorption peaks of the benzene ring's frame vibration were located at 1575, 1352 and 1465 cm^{-1}. The 1036 to 1040 cm^{-1} has a single, crisp band because of (C=S). The HHTA's azomethine (-C=N-) band emerged at 1624 to 1630 cm^{-1}, a wavelength typical of the Schiff base compounds [17].

(Z)-2-hydroxy-2-(4-hydroxyphenyl)-N-(6-thioxo-1,6-dihydropyridin-2-yl)acetimidic acid (HHTA)

Yield: 77 %. M.p. 164 °C; ^{1}H NMR; δH (500 MHz; DMSO-*d6*; 293 K): 4.85 (d, *J* = 5.5 Hz, 1H, C-H of methine group), 5.15 (d, *J* = 5.3 Hz, 1H, O-H attached to methine group), 6.75 - 7.50 (m, dd, t 7H, C-H of two aromatic ring and pyridine-2(1H)-thione group), 9.10 (s, 1H, O-H attached to phenyl group), 12.55 (s, 1H, O-H attached to azomethine group), 13.31 (s, 1H, N-H attached to pyridine-2(1H)-thione group); Elemental analysis: C, 56.51; H, 4.38; N, 10.14; O, 17.37; S, 11.60; IR: Stretching vibration of

the hydroxyl groups was identified as the cause of a large absorption peak at 3430 - 3435 cm^{-1}. The absorption peaks of the benzene ring's frame vibration were located at 1575, 1352, and 1465 cm^{-1}. The 1036 - 1040 cm^{-1} has a single, crisp band because of (C=S). The HHTA's azomethine (-C=N-) band emerged at 1624 to 1630 cm^{-1}, a wavelength typical of the Schiff base compounds.

Electrochemical experiments

The electrochemical experiments were conducted using a Voltalab 40 electronic workstation that was outfitted with a three-electrode system: a platinum electrode that served as the counter electrode, a round C-steel rod that served as the working electrode with a 1 cm^2 exposing area, and a saturated calomel electrode (SCE) that served as the reference electrode. The electrochemical impedance spectroscopy (EIS) test was carried out with an amplitude of 5 mV and a frequency range of 100 kHz to 0.01 Hz after the test system stabilized at the open circuit potential (OCP). The potentiodynamic polarization (PDP) profile was examined at 0.5 mV s^{-1} scanning rate and a voltage open circuit of ±250 mV. Using the VoltMaster 4 in conjunction with the VoltaLab potentiostat workstation 40, the PDP electrochemical kinetics parameters were extracted automatically from the polarization curves via the Tafel line. All samples were washed with distilled water, degreased with an acetone/ethanol mixture, and cleaned with wet emery paper ranging in grade from 200 to 2000 before being used. The electrochemical tests were recorded after three iterations of the experiments conducted under similar circumstances.

Weight loss experiments

Gravimetric weight loss (*W*) tests were conducted in order to validate the rate of corrosion (C_R) and the adsorption of C-steel. Utilized were polished C-steel samples measuring 3×7×0.5 cm. To determine W-loss values, the C-steel specimens were exposed for 12 hours, in addition to and without varying amounts of HAPT and HHTA inhibitors, to the acidic 1 mol L^{-1} HCl electrolyte. The corrosion rate (C_R / g cm^{-2} h^{-1}) was calculated using Equation (1) [18]:

$$C_R = \frac{KW}{StD} \quad (1)$$

where *W* / g, *K*, *t* / h, *S* / cm^2 and *D* / g cm^{-3} stand for the gravimetric weight loss, constant, soaking time, metallic surface area and iron density. Through equations (2) and (3), the surface coverage (θ) and inhibition effectiveness (IE / %) were evalauted.:

$$\theta = \frac{C_R - C_{Rinh}}{C_R} \quad (2)$$

$$IE = 100 \times \theta \quad (3)$$

where C_R and C_{Rinh} denote the corrosion rate in the absence and presence of HAPT and HHTA, respectively. The W-loss results were released after three iterations of the trials under comparable conditions.

Theoretical studies

Density functional theory (DFT) and molecular dynamics (MD) simulations were used in quantum chemical computations employing BIOVIA's Materials-Studio 2017 package [19]. The contact was modelled using a simulation box with periodic boundary conditions, size 2.432×2.432×0.910 nm. To change the Fe (110) surface area and periodicity, it was first built, relaxed, and extended using a supercell. To examine the interactions between the inhibitors under study and the Fe (110) surface, a 3.0 nm vacuum slab was included. The corrosion system was layered after the Fe (110) surface and inhibitor molecules were minimized. To model the actions of HAPT and HHTA agents on the Fe (110) substrate,

the COMPASS force field was employed [20]. For the purpose of running MD simulations, variables such as the imitation time, pressure and temperature were chosen using the discover module.

Results and discussion

EIS measurements

Determining the electrochemical and capacitive behavior of C-steel in a 1 mol L^{-1} HCl acid uninhibited solution, and with HAPT and HHTA inhibitors, was the aim of the EIS investigations. Figure 3 displays the Nyquist plane and Bode graphs for C-steel in an acidic environment, both with and without varying concentrations of HAPT and HHTA inhibitors. The C-steel electrode's Nyquist plots at all inhibitor levels are characterized by depressed single semicircles [21]. Depressed semicircles may be attributed to differences in the electrode surface morphology caused by the roughness and other irregularities. The addition of HAPT and HHTA inhibitors to the corrosive medium results in a considerable increase in the semicircle's diameter. This suggests the adjustments may prevent C-steel surfaces submerged in 1 mol L^{-1} HCl from corroding. This is likely due to the formation of a protection barrier at the C-steel interface, which significantly slows down the corrosion process [22]. The equivalent circuit used to analyze the EIS data was presented in Figure 4, which includes a constant phase element (CPE), solution resistance (R_s), and charge transfer resistance (R_{ct}), in light of the previously discussed results. The apparent presence of a single time constant in the Bode and phase graphs is supported by the observation that only one phase peak exists in the intermediate-frequency region. The existence of a single time constant is supported by the Bode phase charts in Figure 3, which exhibit only one phase bump in the middle frequency band [23]. As shown in Figure 4, the constant phase element (CPE) was utilized instead of the double layer capacitor to give a more precise and representative fit. Equation (4) defines the CPE impedance, $Z_{CPE,}$[24]:

$$Z_{CPE} = \frac{1}{Y_0 (j\omega)^n} \quad (4)$$

where Y_0 represents the CPE factor and j^2 = -1 denotes an imaginary quantity. ω= 2πf (rad s^{-1}) is the angular frequency, and the exponent n denotes the phase shift, which is regarded as the surface inhomogeneity grade. Depending on the value of n, CPE can represent resistance (Y_0 = R) when n = 0, capacitance (Y_0 = C) when n = 1, or Warburg impedance (Y_0 = W) when n = 0.5. After immersing C-steel in the 1 mol L^{-1} HCl solution, the reduced value of n (refer to Table 1) suggested that corrosion-induced metal surface roughening was the cause of surface inhomogeneity.

The observed decrease in surface inhomogeneity after the addition of HAPT and HHTA inhibitors is indicative of the adsorption of the investigated compounds. This also symbolizes a relaxation process brought on by the breakdown of an adsorbate on the C-steel surface, such as the passivation layer, and corrosion inhibitor molecules. The decrease in Y_0 (CPE) values with increasing concentration of HAPT and HHTA inhibitors was explained by a reduction in the local dielectric value and/or an increase in the thickness of the double layer. This shows that by sticking to the C-steel/electrolyte contact, the inhibitor molecules stopped the oxidation of C-steel in the acid solution. At higher levels of the HAPT and HHTA inhibitors, the R_{ct} values increased gradually above the blank solution, suggesting that the inhibitor molecules form a barrier layer that stops corrosive ions from passing across the surface of C-steel. The R_{ct} values can be used to calculate the inhibition efficiency (η_{EIS} / %) by applying Equation (5) [25]:

$$\eta_{EIS} = \left(\frac{R_{ct} - R_{ct}^{\ 0}}{R_{ct}} \right) 100 \quad (5)$$

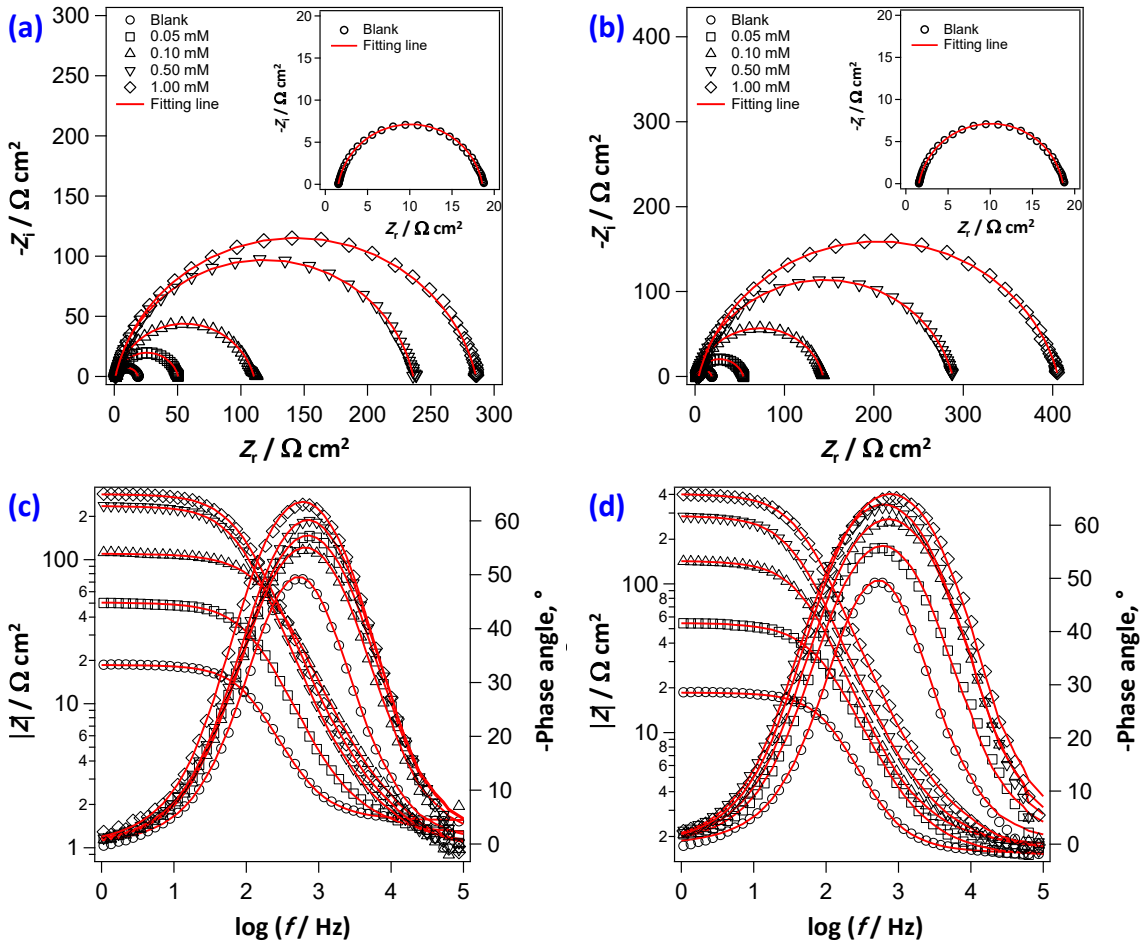

Figure 3. *EIS curves in (a,b) Nyquist, and (c,d) Bode presentation for C-steel in 1 mol L^{-1} HCl solution in the absence and presence of various dosages of HAPT and HHTA inhibitors at 298 K*

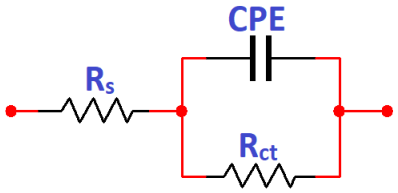

Figure 4. *Equivalent circuit model for EIS fitting results*

Table 1. *EIS data for corrosion of C-steel in 1 mol L^{-1} HCl solution in the absence and presence of various dosages of HAPT and HHTA inhibitors at 298 K*

Inhibitor	C_{inh} / mM	R_s / Ω cm²	CPE		R_{ct} / Ω cm²	C_{dl} / F cm⁻²	$10^{-3}\chi^2$	η_{EIS} / %
			Y_0 / μΩ⁻¹ sⁿ cm⁻²	n				
None	0.00	1.42	312.4	0.89	19.2±0.1	0.928	1.5	—
HAPT	0.05	1.54	221.5	0.88	50.1±2.3	0.355	2.4	61.7
	0.10	1.55	207.1	0.85	113.6±9.6	0.157	3.2	83.1
	0.50	1.49	187.5	0.86	246.2±13.2	0.072	2.8	92.2
	1.00	1.51	155.7	0.84	290.9±12.5	0.061	3.6	93.4
HHTA	0.05	1.50	97.3	0.87	53.9±0.4	0.330	4.1	64.4
	0.10	1.46	105.0	0.84	140.1±1.8	0.127	3.9	86.3
	0.50	1.55	116.6	0.85	295.4±4.7	0.060	4.8	93.5
	1.00	1.56	106.8	0.86	408.5±11.5	0.044	4.6	95.3

R_{ct} and R_{ct}^0, respectively, stand for charge transfer resistance in the presence and absence of the inhibitors under study. At a dosage of 1 mM, Table 1 shows that the inhibition effectiveness of the

HAPT and HHTA inhibitors is 93.4 and 95.3 %, respectively. Moreover, Table 1 demonstrates that the R_{ct} values increase when HAPT and HHTA inhibitors are applied, indicating that the protective layer on the C-steel surface grows. The HHTA inhibitor was shown to be more efficient than the HAPT inhibitor due to the HHTA molecules had an extra two hydroxyl groups, which gave them more adsorption centers [26]. The EIS fitting parameters listed in Table 1 make it evident how the C-steel resistivity has been impacted by the HAPT and HHTA inhibitor dosages. These findings showed that more corrosion inhibitors exist on a flatter C-steel surface, possibly as a result of a barrier created by the HAPT and HHTA inhibitors. The dielectric constant (ε) and the double layer thickness (d) are two electrochemical parameters that are used to determine the double layer capacitance (C_{dl}) values, as per Equation (6) [27]:

$$C_{dl} = \frac{\varepsilon \varepsilon^0}{d} S \quad (6)$$

where ε^0 is the dielectric constant in a vacuum and S is the surface area. The ε values of the inhibited system are clearly very low, indicating that the electron-exchange capabilities were seriously compromised. This demonstrated that the HAPT and HHTA inhibitors successfully displace the pre-adsorbed water fragments by creating a barrier of protection on the C-steel substrate. Y_0 values, however, significantly decreased when the inhibitors were present, suggesting that the pre-adsorbed water molecules on the CS surface quickly replaced the inhibitor molecules.

Potentiodynamic polarization measurements

Potentiodynamic polarization (PDP) studies were performed to learn more about a compound's classification as an anodic, cathodic, or hybrid inhibitor and how it impacted the rate of action of anodic and cathodic processes [28]. Figure 5 illustrates how the dosage of the HAPT and HHTA inhibitors for C-steel in 1 mol L^{-1} HCl acid affected the anodic and cathodic polarization lines at a scan rate of 0.5 mV s^{-1}. Table 2 presents the retrieved properties of electrochemical corrosion of C-steel, such as the effectiveness of inhibition (η_{PDP}), cathodic and anodic Tafel slopes (β_c and β_a), corrosion potential (E_{corr}), and corrosion current density (j_{corr}). To calculate the inhibition effectiveness (η_{PDP} / %), Equation (7) was used [29]:

$$\eta_{PDP} = \left(\frac{i^0_{corr} - i_{corr}}{i^0_{corr}} \right) 100 \quad (7)$$

where the parameters i^0_{corr} and i_{corr} represent the current density of corrosion (mA cm^{-2}) of the working electrode in a 1 mol L^{-1} HCl environment with and without HAPT and HHTA inhibiting agents, respectively. Table 2 illustrates that the presence of HAPT and HHTA inhibitors reduces the density of corrosion currents (j_{corr}) values of C-steel compared to their absence. As increased inhibitor molecules adhere to the C-steel surface, the inhibition efficiency increases as HAPT and HHTA inhibitor concentrations increase. The simultaneously anodic and cathodic current density values decrease with increasing inhibitor doses in 1 mol L^{-1} HCl (see Table 2). Both the anodic and cathodic reactions are slowed down by the presence of HAPT and HHTA. A mixed-type action of the inhibitor is indicated by E_{corr} readings that vary to the cathodic side by around 21.2 to 60.5 mV in relation to the blank, as reported in the literature. By blocking the surface's active sites, HAPT and HHTA inhibitors effectively stop C-steel corrosion in the severe environment of 1 mol L^{-1} HCl, as seen by the symmetrical patterns of polarization curves in the cathodic area of Figure 5. The blocking activity of the HAPT and HHTA inhibitors layer, which covers the C-steel surface, lowers the surface area available for hydrogen atoms (H^+), which lowers the rate of development of hydrogen gas (H_2) [30]. As a result, hydrogen evolution reduction is an activated control and the C-steel reaction mechanism

stays the same. The capacity of HAPT and HHTA inhibitors to protect C-steel from the severe HCl environment is indicated by the anodic Tafel lines in the anodic region. Whereas HAPT and HHTA inhibitors' ability to prevent corrosion at low anodic potential depends on the rate at which they adsorb, creating an adsorbed layer that acts as protection. This indicates that the deterioration of the C-steel electrode at the cathodic and anodic reaction sites was slowed down as a result of the HAPT and HHTA inhibitor molecules adhering to the active sites of the C-steel surface. Significant shifts in β_c values rather than in the values of β_a further supported this conclusion. Examining Figure 5 shows that PDP curves are parallel and comparable when the inhibitors under study are present and absent at varying concentrations. This suggests that the inhibitors prevent metallic corrosion by obstructing the active sites that are present over the surface of the metal without altering the mechanism of C-steel corrosion.

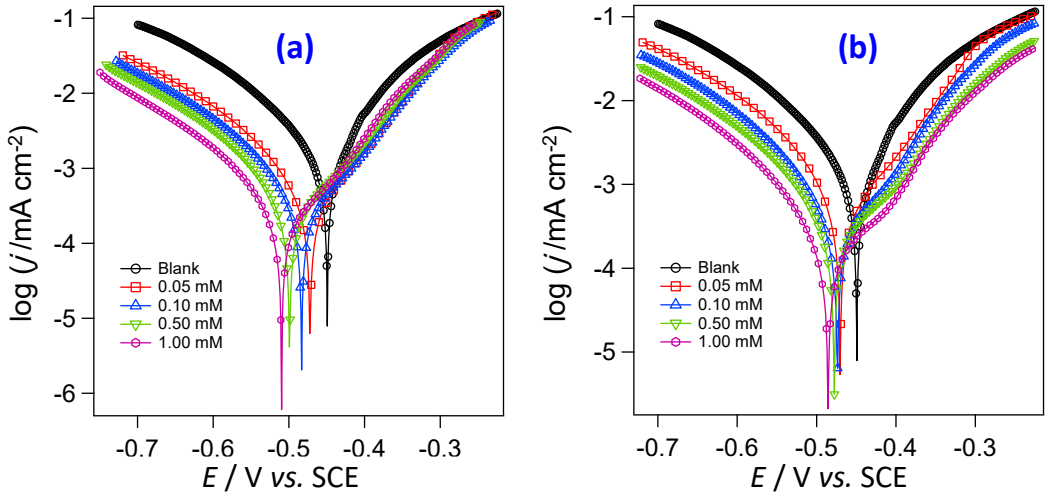

Figure 5. *PDP plots for C-steel in 1 mol L^{-1} HCl solution in the absence and presence of various dosages of (a) HAPT and (b) HHTA inhibitors, at 298 K*

Table 2. *PDP parameters for corrosion of C-steel in 1 mol L^{-1} HCl solution in the absence and presence of various dosages of HAPT and HHTA inhibitors at 298 K*

Inhibitor	C_{inh} / mM	$-E_{corr}$ / V *vs.* SCE	j_{corr} / mA cm^{-2}	β_a / mV dec^{-1}	$-\beta_c$ / mV dec^{-1}	η_{PDP} / %
None	0.00	0.4492	3.64	162	187	—
HAPT	0.05	0.4725	1.40	67	144	61.5
	0.10	0.4831	0.64	78	135	82.3
	0.50	0.4995	0.28	83	142	92.2
	1.00	0.5097	0.24	85	144	93.5
HHTA	0.05	0.4704	1.28	77	133	64.7
	0.10	0.4734	0.54	73	129	85.1
	0.50	0.4776	0.23	71	122	93.6
	1.00	0.4857	0.18	68	124	95.1

This investigation shows that both HAPT and HHTA inhibitors have outstanding corrosion inhibition properties. The HHTA inhibitor structures with two polar hydroxyl group substituents enhance the molecule's interaction with the iron *d*-orbitals at the C-steel surface by utilizing their electrons. The concentration of HAPT and HHTA inhibitors was found to increase the inhibitory efficiency (η_{PDP} / %) to 93.5 and 95.1 % at 1 mM, respectively.

Weight loss measurements

Effect of inhibitor concentration and immersion time

Weight loss (*W*) measurements were a helpful method for analyzing how various inhibitor concentrations affected how quickly the metal in the testing solution dissolved [31]. Figure 6 displays the estimated W-loss parameters. Additionally, Figures 6(a) and (b) illustrate how different HAPT and HHTA inhibitor dosages affect the C-steel surface after being submerged in 1 mol L^{-1} HCl for 12 hours at 298 K.

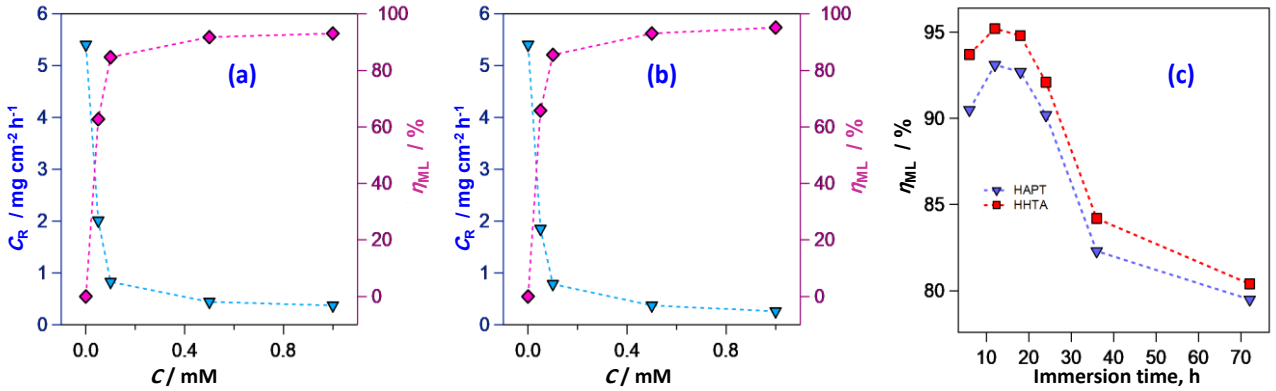

Figure 6. *Dependence of corrosion rate and inhibition efficiency on inhibitor concentration (a) HAPT and (b) HHTA, and (c) relationship of η_{WL} versus immersion time for C-steel in 1 mol L^{-1} HCl solution at 298 K*

Figure 6(a) and (b) clearly show that C-steel shows an improvement in both its corrosion inhibition performance and exterior coverage area with increasing concentrations of HAPT and HHTA inhibitors. By regulating the rate of corrosion, a rise in the concentrations of HAPT and HHTA enhances corrosion inhibition. The fact that the aggressive medium is efficiently isolated from the surface through improving surface coverage and adsorption as the amounts of HAPT and HHTA inhibitors grow may help to explain this phenomenon [32]. This is because, as the concentration of the inhibitor rises, the amount of adsorption on the outer layer of the C-steel increases steadily, forming a thicker and wider protective covering that effectively separates the C-steel from the acidic solution. Consequently, the inhibition efficiency of HAPT and HHTA inhibitors at 1 mM dosage was found to be 93.1 and 95.2 %, respectively, following a 12-hour immersion period. Subsequent investigation confirms that the proposed inhibitors are very stable and very effective. This protective barrier is connected to the molecular makeup of HAPT and HHTA inhibiting agents, involving a ring of aromatic heteroatoms as well as hydroxyl groups, and one or three polar hydroxyl groups in the case of HAPT inhibitor and HHTA inhibitor, respectively [33]. It has been discovered that the HHTA compound works better at adsorbing C-steel than the HAPT compound. This is because the HHTA molecule's active centers have more delocalized electrons.

Immersion time is one of the most crucial variables to take into account when evaluating corrosion prevention. The change in (η_{WL} / %) with the duration of immersion in a 1 mol L^{-1} HCl solution containing 1 mM of HAPT and HHTA inhibitors is displayed in Figure 6(c). With values of 92.7 and 94.8 %, respectively, it was discovered that HAPT and HHTA inhibitors showed an increase in efficiency during 18 hours of immersion. However, after 72 hours of immersion, the HAPT and HHTA inhibitors' respective efficiencies dropped to 79.5 and 80.4 %. The results show that after 18 hours of immersion, a protective coating can fully form on the C-steel framework. This can happen when the electrolytic layer or insulating interface disperses from one side to the other, or when barrier molecules are

absorbed. However, after an extended evaluation period, C-steel may receive additional coverage from the corrosion products that have developed on the metallic surface.

Effect of temperature

Temperature is one important kinetic factor that affects the metallic corrosion and the adsorption of organic molecules on the metallic substrate. Gravimetric tests were conducted at temperatures between 298 and 333 K, both with and without 1 mM of inhibitors for 12 hours of immersion, to demonstrate how temperature affects the corrosion inhibition of HAPT and HHTA inhibitors. It is clear that the corrosion rate (C_r) rose as the temperature rose, and this effect was more noticeable for the blank solution of 1 mol L^{-l} HCl. As a result, inhibitory efficiency varies with temperature, showing that at greater temperatures, dissolution of C-steel dominates HAPT and HHTA adsorption at the metal surface. This is evidenced by a decrease in the adsorption strength across HAPT and HHTA molecules and the C-steel substrate at high temperatures. The activating thermodynamic variables involved in the corrosion process can be derived using the Arrhenius equation (8) and the transition state Equation (9):

$$\ln C_R = \frac{-E_a}{RT} + \ln A \tag{8}$$

$$\ln\left(\frac{C_R}{T}\right) = \frac{-\Delta H_a}{RT} + \left[\ln\left(\frac{R}{N_A h}\right) + \left(\frac{\Delta S_a}{R}\right)\right] \tag{9}$$

where A is the Arrhenius pre-exponential variable, h is Plank's constant, N_A is Avogadro's number, E_a is the activation energy, R is the universal gas constant, T is the absolute temperature, and ΔH_a, ΔS_a are the enthalpy and entropy of activation, respectively. The slope of the ln (C_R) *vs.* 1/T plots of the Arrhenius plot values (Figure 7a) can be used to compute E_a. When HAPT and HHTA were present, the E_a values for C-steel were 69 and 77 kJ mol^{-1}, respectively, whereas the predicted E_a value in blank acid solution was 25 kJ mol^{-1}.

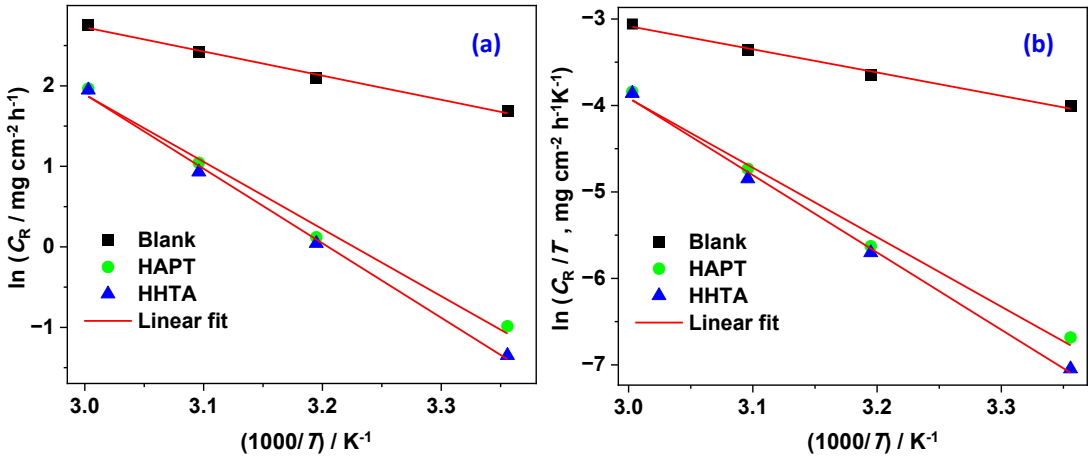

Figure 7. *Arrhenius (a) and transition state (b) plots for C-steel corrosion rates in 1 mol L^{-l} HCl in the absence and presence of 1 mM of HAPT and HHTA*

The higher energy barrier for dissolving C-steel in acid solution is the reason for the higher values of E_a in the presence of HAPT and HHTA molecules. As seen in Figure 7b, the curve of ln (C_R/T) versus 1/T was plotted to determine the values of ΔH_a and $\Delta S_{a'}$. For the dissolution reaction of C-steel, it was discovered that the ΔH_a value is larger when HAPT and HHTA are present (67 and 74 kJ mol^{-1}, respectively) than when they are not (22 kJ mol^{-1}). The endothermic character of the C-steel dissolution process and the sluggish dissolution in the presence of HAPT and HHTA inhibitors

are indicated by the positivity of ΔH_a. For the uninhibited solution, the computed values of ΔS_a were -156 kJ mol^{-1}, whereas the inhibited solution, including HAPT and HHTA inhibitors, had values of -30 and -7 kJ mol^{-1}, respectively. As the reactants are transformed into the activated complexes, the higher negative value of ΔS_a for the uncontrolled solution is typically shown as an increase in disorder. Additionally, this behavior can be explained by the adsorption of HAPT and HHTA molecules on the surface of C-steel, which replaces H_2O molecules [34].

Adsorption isotherm investigations

Adsorption onto the metallic surface is the most common spontaneous action of organic inhibitors under hostile conditions. Adsorption can be classified as either physical (physisorption) or chemical (chemisorption) [35]. The process of physisorption is the delicate unidirectional adsorption of molecule inhibitors on the metal surface, which results from the electrostatic force created by the inhibiting compounds and the metallic charge. During chemisorption, the inhibitor molecules share their charge with unoccupied d-orbitals on the metal surface to establish strong coordination bonds. The interaction between the metallic substance, electrolytic solution, and inhibitory agent determines the type of adsorption [36]. The adsorption types of HAPT and HHTA inhibitors on the C-steel surface in 1 mol L^{-1} HCl were examined using a variety of isotherm equations, including Langmuir, Flory-Huggins, Freundlich, and Temkin isotherms, as presented in Figure 8. To determine how the blocking agent is adsorbed in these circumstances, Langmuir's isotherm was compared to the experimental data, yielding the best fit. As seen in Figure 8, a straight line was drawn across C_{inh}/θ *vs*. C_{inh}-dependence, with a slope of 1.0534 for HAPT and 1.0312 for HHTA, respectively. Equation (10) is a mathematical expression for the Langmuir isotherm [37]:

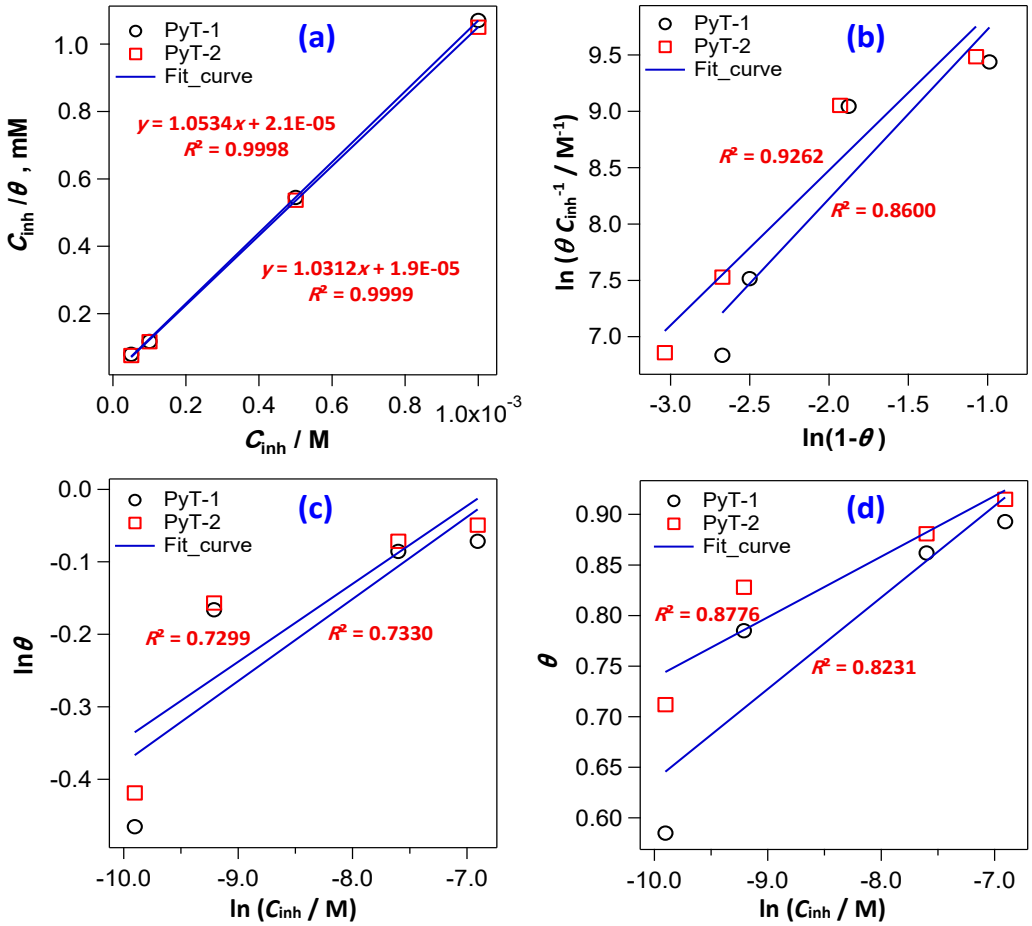

Figure 8. *Different adsorption isotherms (a) Langmuir, (b) Flory-Huggins, (c) Freundlich, and (d) Temkin for C-steel in 1 mol^{-1} HCl solution of various dosages of HAPT and HHTA inhibitors at 298 K*

$$\frac{C_{Inh}}{\theta} = \frac{1}{K_{ads}} + C_{Inh} \quad (10)$$

θ represents the surface coverage, which is computed from the W-loss measurements. K_{ads}, the equilibrium constant of the adsorption reaction, was found to be 47619±11 L mol^{-1} for HAPT and 52632±13 L mol^{-1} for HHTA. These high K_{ads} values suggest that the HAPT and HHTA inhibitor molecules may be able to effectively adsorb over the C-steel surface. Equation (11) connects the K_{ads} and the free energy of adsorption (ΔG^0_{ads}):

$$K_{ads} = \frac{1}{55.5}\exp\left(\frac{-\Delta G^0_{ads}}{RT}\right) \quad (11)$$

where T is the temperature in Kelvin, R is the universal gas constant (8.314 J K^{-1} mol^{-1}) and 55.5 mol denotes the concentration of water in the medium. The adsorption-free energy ΔG^0_{ads} for HAPT and HHTA agents was ultimately found to be -36.6±0.05 and -36.9±0.05 kJ mol^{-1}, respectively. Physisorption happens when the inhibitor-free energy of adsorption is around -20 kJ mol^{-1}, and chemisorption happens when it is about -40 kJ mol^{-1} [38]. This shows that the molecules of HAPT and HHTA inhibitors may firmly adsorb over the surface of C-steel to create a protective layer that stops corrosion and preserves the material.

Quantum chemical calculations

Frontier molecular orbitals calculations

Figure 9 depicts the optimized molecular structures and the charge density distribution of frontier molecular orbitals of synthetic HAPT and HHTA inhibitors. Detailed quantified parameters can be found in Table 3. The HOMO, or highest occupied molecular orbital, signifies the energy level with the highest energy that still contains electrons. This level highlights the regions of the molecule most likely to donate electrons to electrophilic substances.

Table 3. *Theoretical parameters for the neutral and protonated forms of the HAPT and HHTA inhibitors and comparative analysis with similar types of compounds*

Property	HAPT	HHTA	HAPT-H$^+$	HHTA-H$^+$
E_{HOMO} / eV	-4.396	-4.368	-2.675	-3.035
E_{LUMO} / eV	-2.800	-3.224	-2.298	-2.676
ΔE_{gap} / eV	1.596	1.143	0.377	0.358
$I = -E_{HOMO}$ / eV	4.396	4.368	2.675	3.035
$A = -E_{LUMO}$ / eV	2.800	3.224	2.298	2.676
$\chi = (I+A)/2$ / eV	3.598	3.796	2.487	2.855
$\eta = (I-A)/2$ / eV	0.798	0.572	0.189	0.179
$\sigma = 1/\eta$	1.253	1.749	5.300	5.581
$\omega = \chi^2/2\eta$	8.114	12.604	16.388	22.752
ε	0.123	0.079	0.061	0.044
$\Delta N = (\chi_{Fe} - \chi_{inh})/2(\eta_{Fe} + \eta_{inh})$	0.672	0.764	5.785	5.064
$\Delta E = (\chi_{Fe} - \chi_{inh})^2/4(\eta_{Fe} + \eta_{inh})$	0.360	0.334	6.315	4.594
$\omega^+ = (I+3A)^2/16(I-A)$	6.414	10.777	15.168	21.347
$\omega^- = (A+3I)^2/16(I-A)$	10.013	14.574	17.655	24.202
$\Delta\omega^{\pm} = \omega^+ + \omega^-$	16.427	25.351	32.822	45.549
$\Delta E_{Back\text{-}donation} = -\frac{\eta}{4}$	-0.199	-0.143	-0.047	-0.045
μ / D	2.10	2.34	4.14	4.83

Conversely, the LUMO, or lowest unoccupied molecular orbital, represents the lowest energy level without electrons and indicates the areas of the molecule most likely to accept electrons from nucleophilic substances [39]. According to Figure 9, the HOMO is primarily located around the pyridine ring, C=S, and the C=N groups at neutral HAPT and HHTA inhibitors, signifying their function as electron donors. Conversely, the LUMO is predominantly situated on the pyridine ring and most of the substituents on the rings, highlighting its significant electron-accepting effect due to the nitrogen (N^+) of the pyridine ring. These regions in the synthesized inhibitors can interact with the C-steel surface, shielding it from dissolution. On the other hand, HOMO and LUMO have higher orbital density in all the protonated forms, HAPT-H^+ and HHTA-H^+. This suggests that the C=N and C=S groups, pyridine and benzene rings readily accept electrons from Fe orbitals, forming feedback bonds. This means the active centers of the molecules are primarily located in this region.

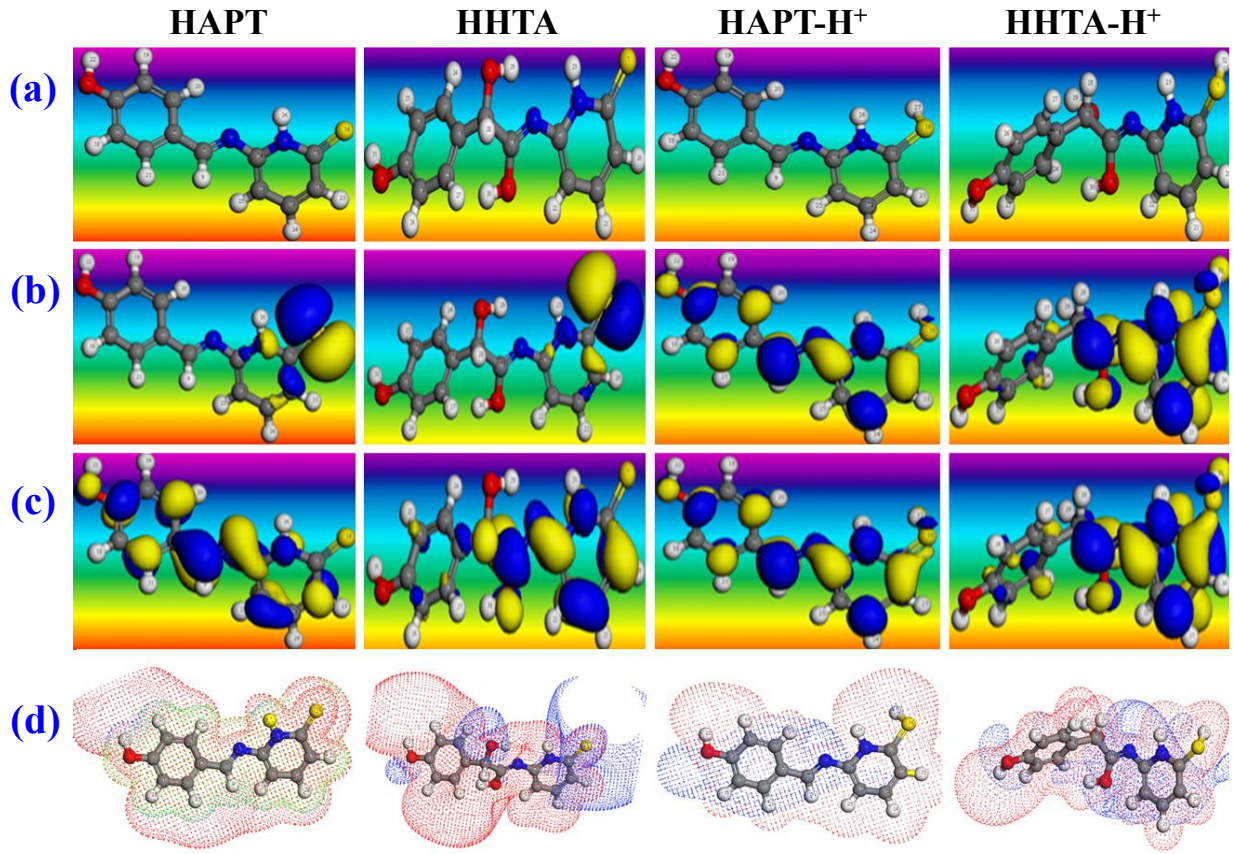

Figure 9. *The frontier molecular orbitals of neutral and protonated forms of the HAPT and HHTA inhibitors: (a) optimized structure, (b) HOMO (c) LUMO and (d) ESP*

As shown in Table 3, HHTA has an E_{HOMO} value of -4.368 eV compared to -4.396 eV for HAPT. Similarly, the E_{LUMO} value for HHTA is -3.224 eV, whereas it is -2.800 eV for HAPT. This implies that HHTA is more efficient in terms of protection than. A smaller energy gap contributes to the chemical stability of the inhibitor, resulting in greater protection efficiency. Table 3 indicates that HHTA has a smaller ΔE_{gap} value of 1.143 eV, compared to 1.596 eV for HAPT, signifying higher stability. Moreover, ΔE_{gap} values for HAPT-H^+ and HHTA-H^+ are 0.377 and 0.358 eV, respectively, confirming the adsorption of protonated molecules on the C-steel surface. Additionally, HHTA exhibits superior inhibition efficiencies due to its lower electronegativity (χ) of 3.796 eV, lower global hardness (η) of 0.572 eV, and higher softness (σ) of 1.749 eV^{-1} compared to HHTA. The dipole moment (μ), which indicates the distribution of electrons within the inhibitor molecule, plays a crucial role in molecular polarization. Strong adsorption of the inhibitor molecule on the metallic substrate is driven by dipole-dipole

interactions, thereby improving corrosion inhibition effectiveness. HHTA shows higher adsorption on metallic substrates due to its higher dipole moment (μ) value of -4.84, indicating greater solubility and polarity than HAPT (-3.98). The ability of an inhibitor molecule to accept and donate electrons is indicated by the electrons transferred fraction ΔN. The number of transferred electrons (ΔN) can be calculated using Equation (12) [40]:

$$\Delta N = \frac{\left(\chi_{Fe} - \chi_{inh}\right)}{2\left(\eta_{Fe} + \eta_{inh}\right)} \tag{12}$$

where χ_{Fe} and χ_{inh} represent the absolute electronegativity of iron and the inhibitor, respectively, and η_{Fe} and η_{inh} represent the absolute hardness of iron and the inhibitor, respectively. Higher ΔN values correlate with greater inhibition efficiencies, making HHTA a more reactive and effective inhibitor than HAPT, with a ΔN value of 0.764 eV compared to 0.672 eV, respectively. If ΔN is positive and less than 3.6 eV, it suggests that the inhibitor molecule is likely to donate electrons to the empty d-orbitals of the Fe metal.

The electrophilicity index (ω) and the nucleophilicity index (ε) are crucial concepts in computational chemistry and molecular reactivity, offering significant insights into how HAPT and HHTA derivative molecules behave in chemical reactions. The electrophilicity index measures a molecule's ability to accept electrons. Electrophilicity is a key parameter for determining how a molecule will act as an electrophile in a chemical reaction. Higher ω values signify a stronger ability to accept electrons, making the molecule a more potent electrophile. This index aids in predicting reaction mechanisms and the reactivity patterns of different molecules. The nucleophilicity index is the reciprocal of the electrophilicity index ($1/\omega$). It provides a measure of a molecule's ability to donate electrons. While electrophilicity focuses on electron acceptance, nucleophilicity emphasizes electron donation [41]. Furthermore, molecules with a lower electrophilicity index are more stable. To identify the most effective corrosion inhibitor following the Minimum electrophilicity principle, we calculated the electrophilicity index values for molecules HAPT and HHTA. Values of ω indicate that the HAPT (8.114) molecule is more stable compared to HHTA (12.604). This suggests that HHTA is a more efficient inhibitor than HAPT, consistent with experimental observations. Additionally, the inhibition efficiencies obtained align well with the inductive effects of the functional groups. On the other hand, the numerical values of the electroaccepting power (ω^+) and electrodonating power (ω^-) of those inhibitors, respectively. offer significant insights into the effectiveness of HAPT and HHTA inhibitors molecules against C-steel corrosion. Table 3 shows that quantum descriptors for the studied molecules clearly indicate that the HHTA molecule consistently has a higher electrodonating power value. The inhibitor adsorption to the C-steel surface increases as the dipole moment (μ) increases. The recorded dipole moments of HAPT and HHTA were found 2.10 and 2.34 D, respectively. The higher dipole moment of the essential compounds of HHTA most likely boosts the efficacy of inhibition and the attachment of the inhibitor. Back donation energy ($\Delta E_{Back\text{-}donation}$) is another parameter linked to the chemical hardness of HAPT and HHTA molecules and can offer valuable information regarding the potential of HAPT and HHTA molecules to inhibit [42]. A molecule with a more negative back-donation energy value will be less effective compared to others. Therefore, the calculated back-donation energy values suggest that HHTA is more suitable for C-steel protection than HAPT. When assessing the performance of HAPT and HHTA inhibitors in preventing corrosion, the interaction energy between C-steel and the inhibitors ΔE is a crucial parameter to consider. Finally, as shown in Table 3, the calculated quantum chemical parameter values for HAPT-H^+ and HHTA-H^+ suggest that the HAPT and HHTA inhibitors adsorb onto the C-steel surface in their protonated forms. Furthermore, the presence of

C=N and C=S groups is intended to improve the effectiveness of the adsorption groups, leading to a denser adhesion to the metal surface [43]. On the other hand, electrostatic potential (ESP) maps serve as essential tools for visualizing the distribution of electric charge within the studied inhibitors. By depicting regions of both positive and negative potential, these maps provide critical insights into the pyridine derivatives' electronic structure, reactivity, and interaction sites. Figure 9d shows the ESP of the neutral and protonated forms of the HAPT and HHTA inhibitors; regions characterized by negative potential (red color) indicate areas of high electron density. These are typically associated with electron-rich sites within the molecule, such as lone pairs on heteroatoms or π-electron clouds in aromatic systems. Such regions of negative potential can also denote nucleophilic sites, which are likely to engage with electrophilic species during chemical reactions. On the other hand, regions displaying positive potential (blue color) signify areas of electron deficiency. These are often located near hydrogen atoms and electron-poor sites within the HAPT and HHTA inhibitor molecules. Positive potential regions are indicative of electrophilic sites, making them prone to interactions with nucleophilic species.

Molecular dynamics simulation

Molecular dynamics (MD) simulation is a strong computational approach used to examine the physical motions of atoms and molecules of the prepared HAPT and HHTA inhibitors and Fe (110) surface over time. MD simulations provide detailed insights into the dynamic behavior of molecular systems at the atomic level. The interaction energy ($E_{interaction}$) of the constructed system was determined using Equation (13) [44]:

$$E_{interaction} = E_{total} - (E_{surface+solution} - E_{inhibitor}) \quad (13)$$

where E_{total} represents the overall energy of the total system under study, $E_{surface+solution}$ denotes the combined energy of the Fe (110) surface and the solution without the presence of the aminopyridine inhibitors, and $E_{inhibitor}$ signifies the energy of the aminopyridine inhibitors. The values of the interaction energy ($E_{interaction}$) for HAPT and HHTA are -418.67 and -418.63 kJ mol^{-1}, respectively. Figure 10 depicts the equilibrium configurations of the neutral and protonated forms of prepared the aminopyridine under study. Figure 10 clearly shows that, during the MD simulation process, the inhibitor molecules gradually moved closer to the Fe (110) surface, ultimately adopting a completely horizontal, flat orientation.

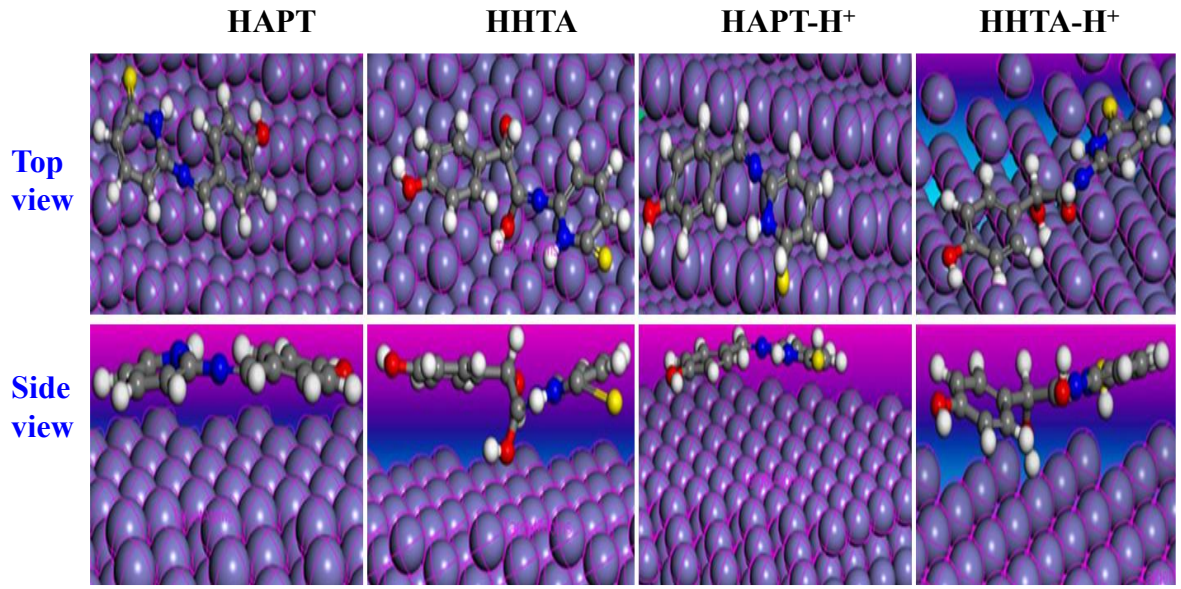

Figure 10. *Top and side views of the neutral and protonated forms of HAPT and HHTA inhibitors adsorption on the Fe (110) surface in MD simulations*

This orientation allows the inhibitor molecules to cover more of the metal surface, thereby achieving high inhibition efficiency. Table 4 shows the molecular dynamic simulation outputs and descriptors of the studied neutral and protonated forms of HAPT and HHTA inhibitors on the Fe (110) surface.

It is evident from Table 4 that greater negative values of adsorption energy of protonated forms of HAPT and HHTA inhibitors signify a stronger and more favorable interaction between the adsorbate and the surface Fe (110), *i.e.* a more stable adsorption process, meaning the HAPT-H^+ and HHTA-H^+ are effectively binding, (E_{bin} = -E_{ads}) to the surface, resulting in effective protection.

Table 4. *Molecular dynamic simulation outputs and descriptors of the studied neutral and protonated forms of HAPT and HHTA inhibitors on the Fe (110) surface*

Molecule/ Descriptors	Energy, kJ mol^{-1}				
	Total	Adsorption	Rigid adsorption	Deformation	Binding
HAPT	-783.721	-415.492	-419.772	4.280	415.492
HHTA	-700.334	-426.310	-449.630	23.320	426.310
HAPT-H^+	-762.169	-435.811	-445.429	9.618	435.811
HHTA-H^+	-748.901	-443.640	-448.777	5.137	443.640

Surface analysis

Figure 11 shows the SEM pictures of polished C-steel surface specimens before and after they were corroded in 1 mol L^{-1} solution of HCl with or without 1 mM of HAPT or HHTA for 12 hours.

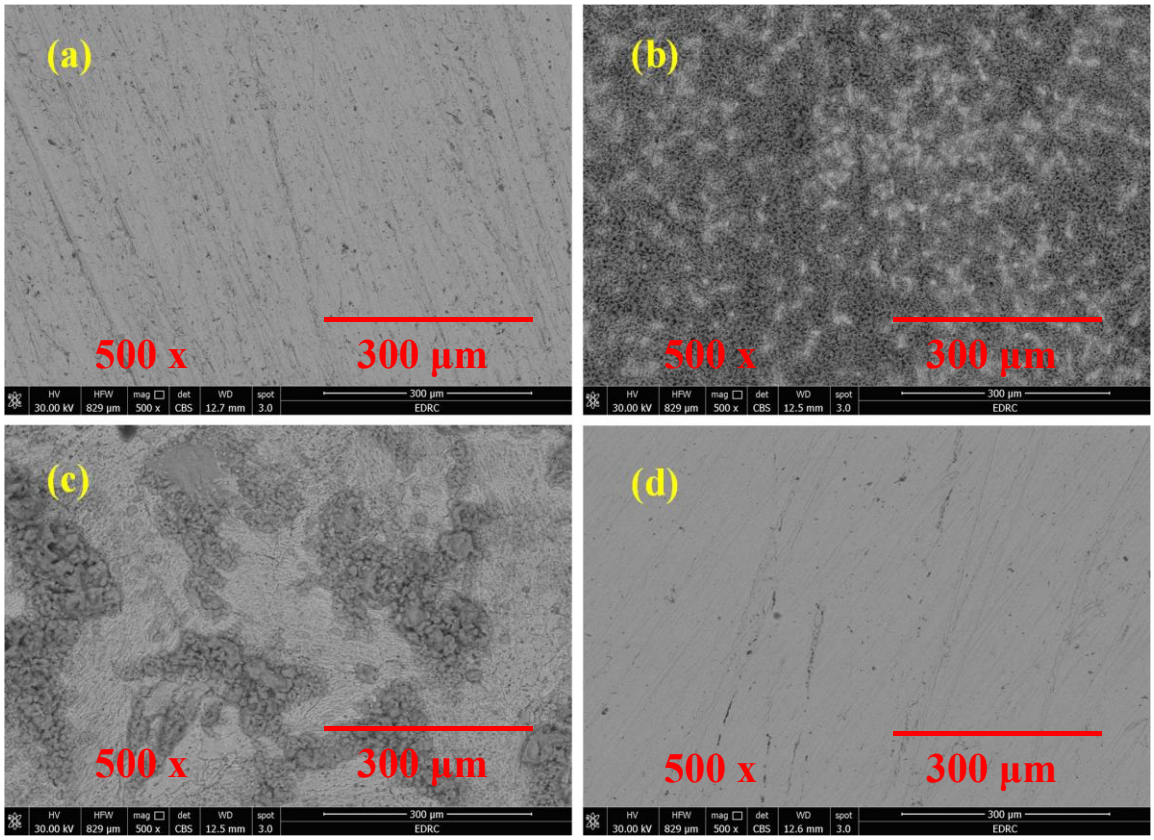

Figure 11. *SEM images of the polished C-steel surface (a) after exposure for 12 h to 1 mol L^{-1} HCl (b), and in the-presence of 1 mM of HAPT (c) and HHTA inhibitor (d)*

As a comparison, the polished C-steel was utilized and shown in Figure 11(a). As shown in Figure 11(b), in the blank acid solution, the C-steel displayed numerous corrosion products and large corrosion holes. The surface of C-steel became flat and smooth after the incorporation of HAPT or

HHTA inhibitor, as illustrated in Figures 11(c) and (d), respectively, with very little corrosion product left behind. This suggests that the incorporation of the aminopyridine inhibitors considerably reduced the corrosion of C-steel. These outcomes align with the results of W-loss studies and electrochemical testing, which show that HAPT and HHTA inhibitors have a more substantial corrosion inhibition impact.

Mechanism of adsorption of HAPT and HHTA

The adsorption of HAPT and HHTA inhibitors onto C-steel has become evident due to their inhibitory potency, as demonstrated by W-loss and electrochemical techniques. Figure 12 provides a general image of the many adsorption strategies the inhibitors investigated here may use to stick to the metal surface. An adsorption isotherm study yielded the ΔG^0_{ads} readings for HAPT and HHTA inhibitors, which are -36.6 and -36.9 kJ mol^{-1}, respectively. This suggests that a mix of physisorption and chemisorption is used by HAPT and HHTA inhibitors to adsorb. These inhibitors can protonate in an acidic environment, which causes pre-adsorbed Cl^- anions to be drawn electrostatically to the surface of C-steel and causes physisorption. Therefore, as the inhibitor molecules are drawn towards the metallic substrate by the electrostatic pull, coordinate covalent bonds start to form, leading to total chemisorption. Both inhibitors contain lone pairs of electrons on the oxygen atoms of the hydroxyl groups, Schiff bases imine moiety (-N=C-), and π-electrons on the phenyl ring. The two additional methoxy groups in HHTA, on the other hand, enhance the electron density. Moreover, the filled orbitals of the iron atoms provide another route by which the electrons could be transferred back to the inhibitor molecule, which is called retro-donation [45]. All these various electron transfer connections among the iron atoms and inhibition molecules form a constant protective layer on the C-steel surface that keeps the metal surface safe from corrosive substances. An electrolyte as powerful as 1 mol L^{-1} HCl would cause significant damage to the metallic surface by oxidizing Fe atoms in the absence of these inhibitors. However, the presence of an inhibitor as potent as HAPT and HHTA inhibitors can significantly delay the anodic, cathodic, or both processes

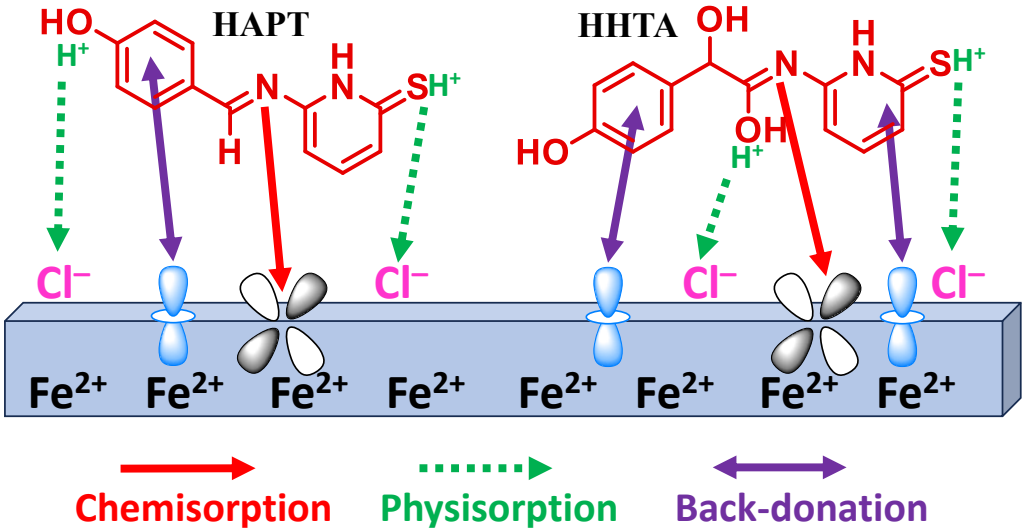

Figure 12. *Schematic illustration showing various adsorption mechanisms by which HAPT and HHTA are adsorbed onto the C-steel substrate*

Some Schiff base inhibiting compounds that have already been investigated for steel alloys corroding in a 1.0 M hydrochloric acid solution are shown in Table 5.

Table 5. *Some Schiff base compounds that are employed as effective corrosion inhibitors for steel alloys in hydrochloric acid solutions*

No.	Schiff base inhibitor	*C* / mM	*η* / %	Ref.
1	(R)-benzyl-2-amino-3-((1-(((2R,3R,4S,5R,6S)-3,4,5-tris(benzyloxy)-6-methoxy-tetrahydro-2H-pyran-2-yl)methyl)-1H-1,2,3-triazol-4-yl)methoxy)propanoate	1.0	92.4	[46]
2	(2R)-benzyl-2-amino-3-((1-(((2R,3R,4S,5R,6S)-3,4,5-tris(benzyloxy)-6-methoxy-tetrahydro-2H-pyran-2-yl)methyl)-1H-1,2,3-triazol-4-yl)methoxy)butanoate		92.1	
3	(2R)-benzyl-2-amino-3-((1-(((2R,3R,4S,5S,6S)-3,4,5-tris(benzyloxy)-6-methoxy-tetrahydro-2H-pyran-2-yl)methyl)-1H-1,2,3-triazol-4-yl)methoxy)butanoate		93.3	
16	4-[(E)-[(2E)-3-(4-nitrophenyl)prop-2-en-1-ylidene]amino]benzenethiol	1.0	64.9	[47]
17	4-[(E)-[(2E)-3-(4-nitrophenyl)prop-2-en-1-ylidene]amino]cyclohexan-1-ol		55.8	
18	benzylidene-pyridine-2-yl-amined	10.0	99.2	[48]
19	(4-benzylidene)-pyridine-2-ylamine		99.4	
20	(4-chloro-benzylidene)-pyridine-2-yl-amine		99.6	
21	2-((5-amino-1,3,4-thiadiazol-2-yl)thio)-N-(benzothiazol-2-yl)acetamide	200*	98.1	[49]
22	2-((5-acetamido-1,3,4-thiadiazol-2-yl)thio)-N-(benzothiazol-2-yl)acetamide		97.3	
27	6,6-(1,4-phenylene)bis(4-oxo-2-thioxo-1,2,3,4-tetrahydropyrimidine-5-carbon itrile)	200*	96.9	[50]
28	6,6 ’-(1,4-phenylene)bis(5-chloro pyrimidine-2,4(1 H,3 H)-dione)		93.3	
32	Boron, nitrogen codoped carbon dots	75*	96.7	[51]
33	(E)-6-((4-hydroxybenzylidene)amino)pyridine-2(1H)-thione (HAPT)	1.0	93.4	Present work
34	(Z)-2-hydroxy-2-(4-hydroxyphenyl)-N-(6-thioxo-1,6-dihydropyridin-2-yl)acetimidic acid (HHTA)		95.2	

*ppm

Conclusion

This study has used both theoretical and experimental methods to investigate the inhibitory behavior of two synthesized Schiff bases, HAPT and HHTA. The following are the conclusions that have been established:

1. According to both theoretical and experimental research, the investigated HAPT and HHTA function well as corrosion inhibitors for C-steel corrosion in 1 mol L^{-1} HCl, and their effectiveness of inhibition rises with concentration.
2. The weight loss data showed that while the corrosion rate increased with temperature, it dramatically decreased as HAPT and HHTA concentrations increased.
3. According to the PDP study's findings, HAPT and HHTA function are mixed-type inhibitors.
4. The EIS investigation found that increasing the HAPT and HHTA dosage increased charge transfer resistance (R_{ct}), indicating significant inhibitory adsorption on the C-steel substrate.
5. HAPT and HHTA adsorb to the C-steel substrate in 1 mol L^{-1} HCl following the Langmuir adsorption isotherm.
6. The SEM study confirmed that the corrosion prevention process was associated with the development of a protective film on the C-steel substrate.
7. In accordance with the experimental results, theoretical studies demonstrated that HHTA was more effective than HAPT.

Acknowledgements*: This research has been funded by Scientific Research Deanship at University of Hail-Saudi Arabia through project number RG-23 188.*

References

[1] B. Liao, Z. Luo, S. Wan, L. Chen, Insight into the anti-corrosion performance of Acanthopanax senticosus leaf extract as eco-friendly corrosion inhibitor for carbon steel in acidic medium, *Journal of Industrial and Engineering Chemistry* **117** (2023) 238-246. https://doi.org/10.1016/j.jiec.2022.10.010

[2] S. Ravi, S. Peters, A. Selvi J, Effect of substitution on corrosion inhibition properties of 4-(substituted fluoro, chloro, and amino) Benzophenone derivatives on mild steel in acidic medium: A combined Electrochemical, surface characterization and theoretical approach, *Journal of the Taiwan Institute of Chemical Engineers* **165** (2024) 105726. https://doi.org/10.1016/j.jtice.2024.105726

[3] R. Kellal, D. Benmessaoud Left, Z.S. Safi, N. Wazzan, O.S. Al-Qurashi, M. Zertoubi, A new approach for the evaluation of liquid waste generated from plant extraction process for the corrosion mitigation of carbon steel in acidic medium: Case of Chrysanthemum Coronarium stems, *Journal of Industrial and Engineering Chemistry* **125** (2023) 370-389. https://doi.org/10.1016/j.jiec.2023.05.046

[4] H. Mohamed; A. A. Farag, B. M. Badran, Corrosion inhibitiob of mild steel using emulsified thiazole adduct in Different binder systems, *Eurasian Chemico-Technological Journal* **10** (2008) 67-77. https://www.researchgate.net/publication/280055435_Corrosion_inhibitiob_of_mild_steel_using_emulsified_thiazole_adduct_in_Different_binder_systems

[5] Z. Song, T. Ye, Y. Zhang, X. Li, L. Jiang, Y. Zhang, H. Cai, M.-Z. Guo, Potential utilization of sludge extract as corrosion inhibitor for reinforcing steel in alkaline environment, *Journal of Industrial and Engineering Chemistry* **136** (2024) 258-273. https://doi.org/10.1016/j.jiec.2024.02.014

[6] A. Toghan, O. K. Alduaij, A. Attia, A. Al Bahir, E. M. Masoud, H. Alhussain, A. M. Eldesoky, A. Farag, A. Fawzy, Exploring the inhibitory performance of expired moxifloxacin and norfloxacin on copper corrosion in saline environment, *Journal of Electrochemical Science and Engineering* **15(3)** (2025) 2464. https://doi.org/10.5599/jese.2646

[7] A.G. Al-Gamal, A.A. Farag, E.M. Elnaggar, K.I. Kabel, Comparative impact of doping nano-conducting polymer with carbon and carbon oxide composites in alkyd binder as anti-corrosive coatings, *Composite Interfaces* **25** (2018) 959-980. https://doi.org/10.1080/09276440.2018.1450578

[8] F. El-Dossoki, S. Abedelhady, M. Abedalhmeed, M. Abdel-Raouf, A. A. Farag, Micellization Properties, Molal Volume and Polarizability of Newly Synthesized Gemini-Cationic Surfactants, *Egyptian Journal of Petroleum* **65** (2021) 585-599. https://doi.org/10.21608/ejchem.2021.71993.4507

[9] A. Toghan, H. Alhussain, A. Attia, O.K. Alduaij, A. Fawzy, A.M. Eldesoky, A. Farag, Corrosion inhibition performance of copper using N-benzylhy-drazinecarbothioamide in a 3.5 % NaCl solution: Original scientific paper, *Journal of Electrochemical Science and Engineering* **14** (2024) 231-245. https://doi.org/10.5599/jese.2181

[10] M.V.L. da Silva, E. de B. Policarpi, A. Spinelli, Syzygium cumini leaf extract as an eco-friendly corrosion inhibitor for carbon steel in acidic medium, *Journal of the Taiwan Institute of Chemical Engineers* **129** (2021) 342-349. https://doi.org/10.1016/j.jtice.2021.09.026

[11] A.A. Farag, A. Toghan, M.S. Mostafa, C. Lan, G. Ge, Environmental Remediation through Catalytic Inhibition of Steel Corrosion by Schiff's Bases: Electrochemical and Biological Aspects, *Catalysts* **12** (2022) 838. https://doi.org/10.3390/catal12080838

[12] K.R. Ansari, M.A. Quraishi, Bis-Schiff bases of isatin as new and environmentally benign corrosion inhibitor for mild steel, *Journal of Industrial and Engineering Chemistry* **20** (2014) 2819-2829. https://doi.org/10.1016/j.jiec.2013.11.014

[13] A. Toghan, A. Fawzy, A.I. Alakhras, A.A. Farag, Electrochemical and Theoretical Examination of Some Imine Compounds as Corrosion Inhibitors for Carbon Steel in Oil Wells Formation Water, *International Journal of Electrochemical Science* **17** (2022) 2212108. https://doi.org/10.20964/2022.12.94

[14] W. Ettahiri, G. Al Ati, R. Salim, K. Chkirate, B. Hammouti, R. Achour, Z. Rais, A. Baouid, E.M. Essassi, M. Taleb, Synthesis and characterization of pyrazole-acetamide Schiff bases as

highly effective inhibitors for mild steel in 1 M HCl, *Journal of Industrial and Engineering Chemistry* **140** (2024) 545-555. https://doi.org/10.1016/j.jiec.2024.06.013
[15] F. Mohamadpour, 2-Aminopyridine as a recyclable catalyst for metal-free synthesis of pyrano [2,3-d]pyrimidine scaffolds, *Current Research in Green and Sustainable Chemistry* **10** (2025) 100444. https://doi.org/10.1016/j.crgsc.2024.100444
[16] H. Jafari, E. Ameri, M. Hassan Vakili, A. Berisha, Effect of OH position on adsorption behavior of Schiff-base derivatives in corrosion inhibition of carbon steel in 1 M HCl, *Electrochemistry Communications* **159** (2024) 107653. https://doi.org/10.1016/j.elecom.2023.107653
[17] A.A. Altalhi, E.A. Mohammed, S.S.M. Morsy, N.A. Negm, A.A. Farag, Catalyzed production of different grade biofuels using metal ions modified activated carbon of cellulosic wastes, *Fuel* **295** (2021) 120646. https://doi.org/10.1016/j.fuel.2021.120646
[18] K. Haruna, T.A. Saleh, Dopamine functionalized graphene oxide (DGO) as a corrosion inhibitor against X60 carbon steel corrosion in a simulated acidizing environment; An electrochemical, weight loss, SERS, and computational study, *Surfaces and Interfaces* **44** (2024) 103688. https://doi.org/10.1016/j.surfin.2023.103688
[19] BIOVIA Materials Studio, Dassault Systèmes, https://www.3ds.com/products/biovia/materials-studio
[20] COMPASS force field, SklogWiki, http://www.sklogwiki.org/SklogWiki/index.php/COMPASS_force_field
[21] J. He, X. Li, B. Xie, Y. He, C. Lai, B. Dou, J. Feng, M. Liu, R. Ji, W. Zhao, Exploration of rigid double Schiff base with a symmetrical plane as highly effective corrosion inhibitor for mild steel in hydrochloric acid environment: Experimental and theoretical approaches, *Materials Chemistry and Physics* **313** (2024) 128785. https://doi.org/10.1016/j.matchemphys.2023.128785
[22] R. Khanna, M. Dudi, B. Mangla, V. Kalia, A. Sihmar, H. Tanwar, H. Dahiya, Assessment of pyrazole Schiff base's corrosion inhibition effectiveness incorporating oxadiazole moiety on mild steel in 1 M HCl: A holistic theoretical and experimental analysis, *Journal of Molecular Structure* **1317** (2024) 139066. https://doi.org/10.1016/j.molstruc.2024.139066
[23] M. Sharma, S. Singh Yadav, P. Sharma, L. Yadav, M. Zainul Abedeen, H. Singh Kushwaha, R. Gupta, An experimental and theoretical investigation of corrosion inhibitive behaviour of 4-amino antipyrine and its schiff's base (BHAP) on mild steel in 1 M HCl solution, *Inorganic Chemistry Communications* **157** (2023) 111330. https://doi.org/10.1016/j.inoche.2023.111330
[24] S. Boukazoula, D. Haffar, R. Bourzami, L. Toukal, V. Dorcet, Synthesis, characterizations, crystal structure, inhibition effects and theoretical study of novel Schiff base on the corrosion of carbon steel in 1 M HCl, *Journal of Molecular Structure* **1261** (2022) 132852. https://doi.org/10.1016/j.molstruc.2022.132852
[25] M. Chen, S. Chen, J. Pi, S. Chen, Q. Wang, C. Fu, An investigation of modified dialdehyde starch as a highly efficient green corrosion inhibitor for carbon steel in 1 M HCl medium: Synthesis, experimental and theoretical studies, *Industrial Crops and Products* **215** (2024) 118534. https://doi.org/10.1016/j.indcrop.2024.118534
[26] A. Toghan, A. Fawzy, A.I. Alakhras, M.M.S. Sanad, M. Khairy, A.A. Farag, Correlating Experimental with Theoretical Studies for a New Ionic Liquid for Inhibiting Corrosion of Carbon Steel during Oil Well Acidification, *Metals* **13** (2023) 862. https://doi.org/10.3390/met13050862
[27] H.T. Obaid, M.Y. Kadhum, A.S. Abdulnabi, Azo Schiff base derived from 2-hydroxy-1-naphthaldehyde as corrosion inhibitors for carbon steel in HCl medium: Experimental and theoretical studies, *Materials Today: Proceedings* **60** (2022) 1394-1401. https://doi.org/10.1016/j.matpr.2021.10.380
[28] H. Jafari, E. Ameri, M.H. Vakili, A. Berisha, Novel Silicon-based schiff-base as corrosion inhi-

bitor for anti-corrosion behavior of API 5L Grade B in 1M HCl, *Materials Chemistry and Physics* **311** (2024) 128499. https://doi.org/10.1016/j.matchemphys.2023.128499

[29] H.M. Kasim Sheit, S.M. Kani, M.A. Sathiq, S.S.S. Abuthahir, K.S. Mohan, S.B. Mary, K. V Gunavathy, Investigations on the effect of 2-[(furan-3ylmethylene)-amino]-benzenethiol on corrosion in carbon steel, *Results in Surfaces and Interfaces* **12** (2023) 100143. https://doi.org/10.1016/j.rsurfi.2023.100143

[30] P. Wang, Y. Song, L. Fan, Z. Li, K.R. Ansari, M. Talha, A. Singh, Y. Lin, Anticorrosion evaluation of novel Schiff-Imidazole molecules for Q235 steel in 1.0 mol/L HCl by computational and experimental methodologies, *Journal of Molecular Structure* **1306** (2024) 137793. https://doi.org/10.1016/j.molstruc.2024.137793

[31] D.N. Bima, H. Muhtar, A. Darmawan, Comprehensive investigation of a new pyrazole derivative Schiff base complex: Revealing its potent protection against carbon steel corrosion, *Chemical Engineering Research and Design* **208** (2024) 313-325. https://doi.org/10.1016/j.cherd.2024.06.043

[32] L.B. Furtado, R.C. Nascimento, F.J.F.S. Henrique, M.J.O.C. Guimarães, J.C. Rocha, J.A.C. Ponciano, P.R. Seidl, Effects of temperature, concentration and synergism on green Schiff bases synthesized from vanillin in applications as corrosion inhibitors for carbon steel in well stimulation, *Journal of Petroleum Science and Engineering* **213** (2022) 110401. https://doi.org/10.1016/j.petrol.2022.110401

[33] Z.I. Jasim, K.H. Rashid, K.F. AL-Azawi, A.A. Khadom, Optimization of the corrosion inhibition performance of novel oxadiazole thione-based Schiff base for mild steel in HCl media using Doehlert experimental design, *Inorganic Chemistry Communications* **160** (2024) 111911. https://doi.org/https://doi.org/10.1016/j.inoche.2023.111911

[34] X. Li, L. Chen, B. Xie, C. Lai, J. He, J. Feng, Y. Yang, R. Ji, M. Liu, Two semi flexible nonplanar double Schiff bases as corrosion inhibitors for mild steel in HCl solution: Experimental and theoretical investigations, *Journal of Environmental Chemical Engineering* **11** (2023) 110077. https://doi.org/10.1016/j.jece.2023.110077

[35] X. Li, S. Deng, G. Du, X. Xie, Synergistic inhibition effect of walnut green husk extract and sodium lignosulfonate on the corrosion of cold rolled steel in phosphoric acid solution, *Journal of the Taiwan Institute of Chemical Engineers* **114** (2020) 263-283. https://doi.org/10.1016/j.jtice.2020.09.010

[36] L. Guo, L. Zhu, S. Kaya, R. Sun, A.G. Ritacca, K. Wang, J. Chang, Electrochemical and surface investigations of N, S codoped carbon dots as effective corrosion inhibitor for mild steel in acidic solution, *Colloids and Surfaces A: Physicochemical and Engineering Aspects* **702** (2024) 135062. https://doi.org/10.1016/j.colsurfa.2024.135062

[37] X.-L. Li, B. Xie, C. Lai, J.-S. Feng, X.-Q. Liu, L. Chen, Y.-G. Yang, R.-W. Ji, J.-Y. He, W. Li, M.-N. Liu, Adsorption and corrosion inhibition performance of two planar rigid pyridinecarboxaldehyde-based double Schiff bases for mild steel in HCl solution: Experimental and computational investigations, *Journal of Molecular Liquids* **355** (2022) 118926. https://doi.org/10.1016/j.molliq.2022.118926

[38] A.A. Farag, Oil-in-water emulsion of a heterocyclic adduct as a novel inhibitor of API X52 steel corrosion in acidic solution, *Corrosion Reviews* **36** (2018) 575-588. https://doi.org/10.1515/corrrev-2018-0002

[39] H. Hamani, D. Daoud, S. Benabid, T. Douadi, Electrochemical, density functional theory (DFT) and molecular dynamic (MD) simulations studies of synthesized three news Schiff bases as corrosion inhibitors on mild steel in the acidic environment, *Journal of the Indian Chemical Society* **99** (2022) 100492. https://doi.org/10.1016/j.jics.2022.100492

[40] M.M. Hegazy, E.M. Khalil, E. Badr, M.A.F. Mansour, Amino pyridine derivatives as new corrosion inhibitors for protection cabling metal of crude oil well during acidizing, *Egyptian*

Journal of Petroleum **32** (2023) 8-20. https://doi.org/10.1016/j.ejpe.2023.08.003
[41] S. Kaya, F. Siddique, D.O. Isin, K.P. Katin, V. Asati, A. Berisha, Inhibition performances of new pyrazole derivatives against the corrosion of C38 steel in acidic medium: Computational study, *Results in Surfaces and Interfaces* **14** (2024) 100184. https://doi.org/10.1016/j.rsurfi.2024.100184
[42] A.H.J. Mofidabadi, G. Bahlakeh, B. Ramezanzadeh, Fabrication of a novel hydrophobic anti-corrosion film based on Eu2O3/stearic acid on steel surface; Experimental and detailed computer modeling studies, *Journal of the Taiwan Institute of Chemical Engineers* **114** (2020) 228-240. https://doi.org/10.1016/j.jtice.2020.09.022
[43] F.E.L. Hajjaji, R. Salim, E. Ech-chihbi, A. Titi, M. Messali, S. Kaya, B. El Ibrahimi, M. Taleb, New imidazolium ionic liquids as ecofriendly corrosion inhibitors for mild steel in hydrochloric acid (1 M): Experimental and theoretical approach, *Journal of the Taiwan Institute of Chemical Engineers* **123** (2021) 346-362. https://doi.org/10.1016/j.jtice.2021.05.005
[44] C. Boulechfar, H. Ferkous, S. Djellali, M.A. Amin, S. Boufas, A. Djedouani, A. Delimi, Y. Ben Amor, K. Kumar Yadav, B.-H. Jeon, Y. Benguerba, DFT/molecular scale, MD simulation and assessment of the eco-friendly anti-corrosion performance of a novel Schiff base on XC38 carbon steel in acidic medium, *Journal of Molecular Liquids* **344** (2021) 117874. https://doi.org/10.1016/j.molliq.2021.117874
[45] N. El Guesmi, B.H. Asghar, M.I. Awad, A.N. Al Harbi, M.A. Kassem, M.R. Shaaban, Novel thiazole-derived Schiff-Bases as efficient corrosion inhibitors for mild steel in acidic Media: Synthesis, electrochemical and Computational insights, *Arabian Journal of Chemistry* **17** (2024) 105867. https://doi.org/10.1016/j.arabjc.2024.105867
[46] Q. Deng, N.-N. Ding, X.-L. Wei, L. Cai, X.-P. He, Y.-T. Long, G.-R. Chen, K. Chen, Identification of diverse 1,2,3-triazole-connected benzyl glycoside-serine/threonine conjugates as potent corrosion inhibitors for mild steel in HCl, *Corrosion Science* **64** (2012) 64-73. https://doi.org/10.1016/j.corsci.2012.07.001
[47] O.A. Odewole, C.U. Ibeji, H.O. Oluwasola, O.E. Oyeneyin, K.G. Akpomie, C.M. Ugwu, C.G. Ugwu, T.E. Bakare, Synthesis and anti-corrosive potential of Schiff bases derived 4-nitrocinnamaldehyde for mild steel in HCl medium: Experimental and DFT studies, *Journal of Molecular Structure* **1223** (2021) 129214. https://doi.org/10.1016/j.molstruc.2020.129214
[48] H. Ashassi-Sorkhabi, B. Shaabani, D. Seifzadeh, Corrosion inhibition of mild steel by some Schiff base compounds in hydrochloric acid, *Applied Surface Science* **239** (2005) 154-164. https://doi.org/10.1016/j.apsusc.2004.05.143
[49] K. Keshar, R.K. Mitra, S.K. Gupta, P. Kumari, I. Ahmad, I.B. Obot, A.H. Alamri, M. Yadav, Corrosion inhibition and adsorption behaviour of benzothiazole compounds on mild steel in an acidic environment: Experimental and theoretical approach, *Colloids and Surfaces A: Physicochemical and Engineering Aspects* **711** (2025) 136318. https://doi.org/10.1016/j.colsurfa.2025.136318
[50] R.K. Mehta, S.K. Gupta, M. Yadav, Studies on pyrimidine derivative as green corrosion inhibitor in acidic environment: Electrochemical and computational approach, *Journal of Environmental Chemical Engineering* **10** (2022) 108499. https://doi.org/10.1016/j.jece.2022.108499
[51] V. Saraswat, T.K. Sarkar, N. Sandhu, S. Kohli, M. Rawat, K. Keshar, M. Yadav, N. Bano, Mechanistic Insights into the Corrosion Inhibition Performance of Eco-Friendly Nitrogen and Boron Co-Doped Carbon Dots for Mild Steel in a 15% HCl Solution, *Langmuir* **41** (2025) 3528-3540. https://doi.org/10.1021/acs.langmuir.4c04672